

Upper tropospheric humidity from SAPHIR on-board Megha-Tropiques

Nizy Mathew¹, Viju Oommen John²,
C. Suresh Raju^{1,*} and K. Krishna Moorthy³

¹Space Physics Laboratory, Vikram Sarabhai Space Centre,
Indian Space Research Organization,
Thiruvananthapuram 695 022, India

²Hadley Centre, Met Office, Exeter, UK

³ISRO Headquarters, Antariksh Bhavan, New BEL Road,
Bengaluru 560 231, India

Upper tropospheric humidity (UTH) has been derived using a ‘brightness temperature (T_b) transformation’ method from the humidity sounder channels of SAPHIR payload on-board Megha-Tropiques (MT). These channels are very close to the water vapour absorption peak at 183.31 GHz. The channel at 183.31 ± 0.2 GHz enables retrieval of humidity up to the highest altitude possible with the present nadir-looking microwave humidity sounders. Megha-Tropiques satellite has an equatorially inclined orbit, which ensures frequent spatial and temporal coverage of the global tropical belt. Transformation coefficients for the first three channels for all the incidence angles have been derived and are used to convert brightness temperatures to weighted average upper tropospheric humidity having weighting function peaks at different pressure levels. The methodology has been validated by comparing the SAPHIR-derived UTH with that derived from radiosonde observations. Inter-comparison of the derived UTH has been done with layer averaged humidity product from SAPHIR measurements and with UTH product using infrared measurements from Kalpana satellite (MOSDAC). UTH over the tropical belt for six months has been studied taking the advantage of the humidity product with high spatial and temporal resolution. The transformation coefficients and methodology to identify the cloud-free pixels to derive UTH from the three channels for all the possible incidence angles are presented here, so that the users can directly derive UTH from the brightness temperature data.

Keywords: Brightness temperature, radiosonde observations, sounder channels, upper tropospheric humidity.

Water vapour is a critical greenhouse gas in the atmosphere, which plays an important role in the energy budget and in the formation of clouds. In particular, the distribution of free tropospheric humidity over the inter-tropical belt has been identified as an important contributor to the water vapour feedback in global warming¹. The importance of upper tropospheric humidity (UTH) in the Earth’s radiation budget has been well illustrated². Radiosonde measurements of humidity are sparse and tend to have problems under highly dry conditions. In this context,

satellite-based measurements have the advantage of providing tropospheric humidity globally. Infrared sounders on different platforms can provide information on humidity under cloud-free conditions³, but microwave sounders have the advantage of all-sky sampling.

Soden and co-workers^{4,5} have developed an interpretation tool which provides a convenient means of interpreting the observed infrared radiance at 6.7 μm channel in terms of upper tropospheric humidity, which is the weighted average of relative humidity in a layer from ~200 to 500 hPa. Buehler *et al.*^{6,7} have derived the Jacobian weighted mean relative humidity of the upper troposphere using the 183.31 ± 1.0 GHz channel of the Advanced Microwave Sounding Unit-B (AMSU-B) on-board NOAA operational satellites and obtained daily maps of UTH to generate the climatology of UTH over the globe. AMSU-derived UTH has been used to study humidity variability associated with the Indian summer monsoon⁸. In the present communication, brightness temperature measurements of the first three channels (183.31 ± 0.2 , 183.31 ± 1.1 and 183.31 ± 2.8 GHz) of the SAPHIR humidity sounder on-board Megha-Tropiques (MT) have been used to derive Jacobian weighted mean UTH for three layers. The transformation coefficients for these three channels for all possible incidence angles and the methodology to find cloud-free pixels are also presented here, to help the users to directly derive UTH from SAPHIR brightness temperature data.

Unlike its predecessors such as SSM/T2 or AMSU-B, SAPHIR sounder is able to provide humidity information above up to ~200 hPa using its 183.31 ± 0.2 GHz channel. It is a unique humidity sounder in terms of its number of channels, spatial resolution and coverage over the global tropical belt. The low inclination orbit with revisits at different local times of MT helps to capture the weather-related atmospheric variability. SAPHIR sounds at six frequencies around 183.31 GHz water vapour absorption line are listed in Table 1. This instrument has an improved spatial resolution (10 km) compared to similar instruments in other satellites. Maximum scan angles of SAPHIR are limited to around ~43°, whereas those for AMSU-B are ~48°.

Layer averaged humidity products are made available in the MOSDAC website (<http://mosdac.gov.in>). However, MOSDAC does not provide the Jacobian weighted

Table 1. SAPHIR channels and frequencies

Channel no.	Frequency (GHz)	Band width (MHz)
S1	183.31 ± 0.2	200
S2	183.31 ± 1.1	350
S3	183.31 ± 2.8	500
S4	183.31 ± 4.2	700
S5	183.31 ± 6.8	1200
S6	183.31 ± 11.0	2000

*For correspondence. (e-mail: c_sureshraj@vssc.gov.in)

humidity (UTH) from SAPHIR channels, which is direct transformation of brightness temperature (T_b) to humidity in the upper troposphere. The present UTH products manifest all the atmospheric humidity variability, irrespective of being over land or the ocean.

The transformation coefficients to convert brightness temperature measurements to UTH are derived for the first three channels (183.31 ± 0.2 , 183.31 ± 1.1 and 183.31 ± 2.8 GHz) for each incidence angle⁷. The weighted mean upper tropospheric humidity was derived using these coefficients from the brightness temperature measurements of SAPHIR for the period July–December 2012. Preliminary results from the analysis of the data are presented here. The present communication presents the characteristics of the Megha-Tropiques satellite and the humidity sensor SAPHIR, and describes other datasets used in the study. This is followed by a brief description of the methodology used to derive humidity, validation of UTH with different humidity measurements and an inter-comparison with other humidity products. Then the results of the study are presented as well as the conclusion. Appendix presents the transformation coefficients ([Table S1; see Supplementary Material online](#)).

The Megha-Tropiques is a joint venture of the Indian Space Research Organization (ISRO) and the Centre National d'Etudes Spatiales (CNES), France, designed to study the tropical moisture and energy budget^{1,9}. The satellite boards four payloads, namely SAPHIR (Sondeur Atmosphérique du Profil d'Humidité Inter-tropical par Radiométrie), MADRAS (Microwave Analysis and Detection of Rain and Atmospheric Structures), SCARAB (Scanner for Radiation Budget) and ROSA (Radio Occultation Sensor for Atmosphere). Among these, MADRAS and SAPHIR are operated in the microwave regime to study the characteristic features of tropical weather systems such as cloud microphysics, precipitation, ocean surface winds, total water vapour and liquid water content. The 11-channel microwave imager MADRAS measures the upwelling irradiance at six different frequencies in the range 18.7–157 GHz (ref. 10). The data from MADRAS are also used to characterize the terrain and estimate microwave land surface emissivity¹¹. SAPHIR is a millimetre waves sounder designed to study the tropical convective systems as well as the altitude profiles of tropospheric humidity. It is a cross-track scanning radiometer and the incidence angles near nadir are $\sim 0.27^\circ$ and 50.4° for the outermost pixels. There are 182 pixels on a single scan line. The radiometer sensitivity varies from ≤ 1 K for a bandwidth of ≤ 2 GHz to 2 K for 200 MHz and the calibration accuracy is ≤ 2 K (ref. 12). The sample size along the track varies from 10 to 15 km and across track from 10 to 23 km. The present study makes use of the brightness temperature (level-1 A1) data obtained from SAPHIR released by ISRO (<http://mosdac.gov.in>) In Table 2, the general sensor features of SAPHIR are compared with those of AMSU-B.

In addition to the SAPHIR brightness temperature data, radiosonde measurements (<http://weather.uwyo.edu/upperair/sounding.html>) are used for validation. UTH product derived from the infrared measurements by Very High Resolution Radiometer (VHRR) on-board Kalpana satellite (Kalpana UTH) and SAPHIR layer averaged humidity product (<http://mosdac.gov.in>) is used for the inter-comparison of SAPHIR UTH in the present study.

Humidity Jacobians (K_{ij}) for the first three frequency channels (i) for each incidence angle are derived as a function of altitude (j) by providing the Chevallier profiles¹³, which cover a wide range of atmospheric temperature T_j and relative humidity RH_j , as input to the radiative transfer model ARTS (Atmospheric Radiative Transfer Simulator)¹⁴. The ARTS model has been validated against a range of models¹⁵. Weighted mean relative humidity is then calculated for each profile using the relation

$$UTH_j(\theta) = \frac{\sum_j K_{ij}(\theta)RH_j}{\sum_j K_{ij}(\theta)}. \quad (1)$$

Brightness temperatures (T_b) are also simulated for each profile at each frequency–incidence angle combination using ARTS. From the regression relation

$$\ln(UTH) = a + bT_b. \quad (2)$$

Two linear fit parameters a and b are derived for the transformation of brightness temperatures to UTH. Figure 1 shows the Jacobians for the three channels used (for a typical tropical profile).

The derived coefficients are used to retrieve Jacobian weighted UTH from SAPHIR brightness temperature observations. The transformation parameters a and b for the three channels and for different SAPHIR incidence angles are listed in Appendix ([Table S1, see Supplementary Material online](#)). Pixels affected by deep convective clouds are identified using the brightness temperature difference method^{16,17}, and these pixels are discarded. The part of the UTH error resulting only from radiometric

Table 2. General features of SAPHIR and AMSU-B

Features	SAPHIR	AMSU-B
Orbital inclination ($^\circ$)	20	98
No. of sounding channels	6	3
Swath width (km)	~ 2060	~ 2300
No. of pixels/scan line 1	82	90
Maximum incidence angle ($^\circ$)	50.4	58.5
IFOV ($^\circ$)	0.47	1.1
Pixel size across track (km)	10–23	20–64
Pixel size along track (km)	10–15	16–27

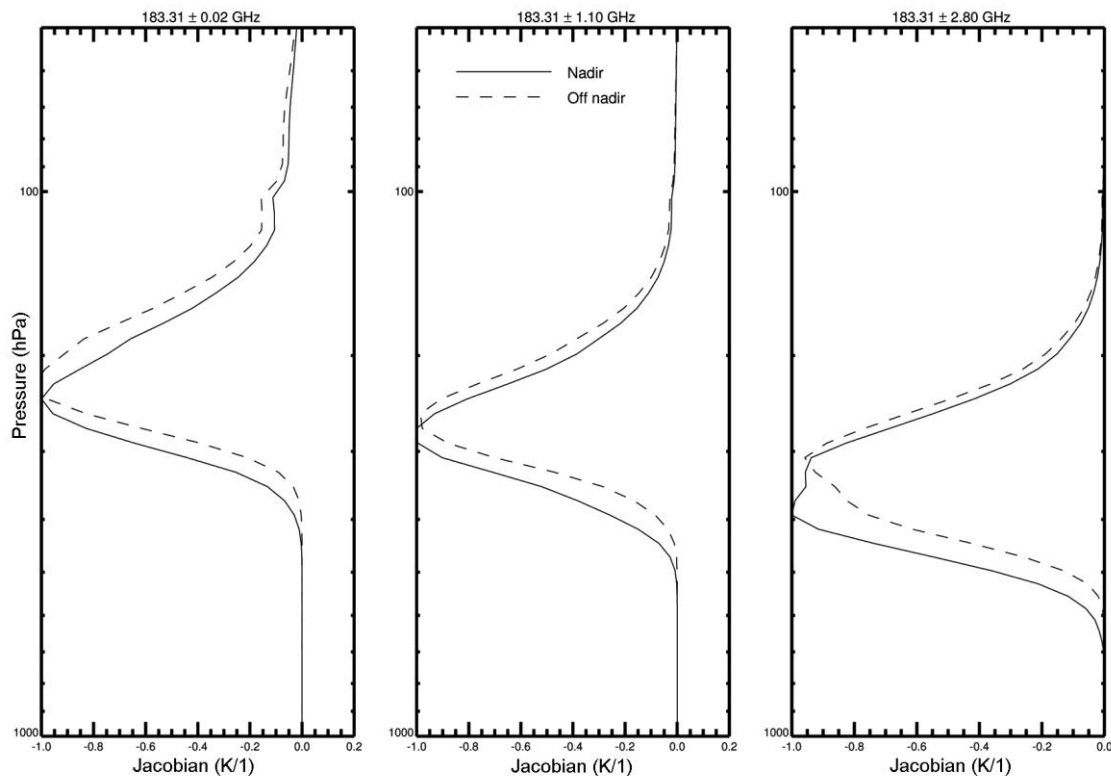


Figure 1. Humidity Jacobians for a tropical situation.

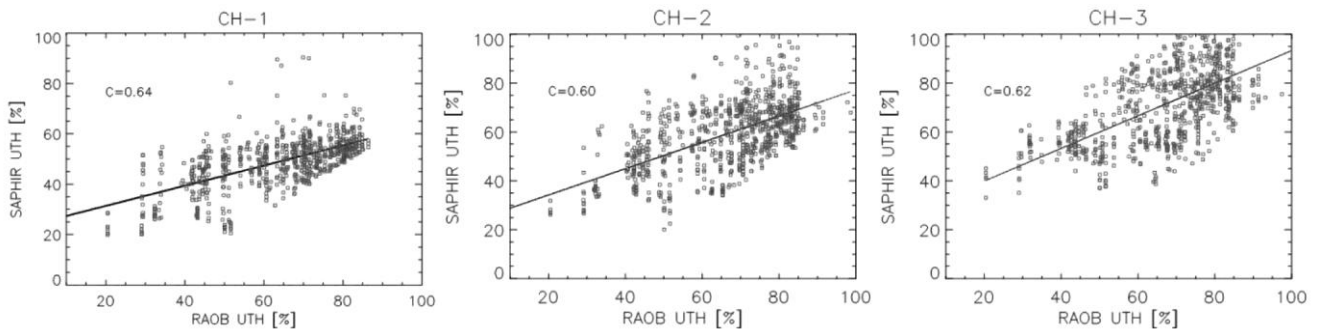


Figure 2. Comparison of UTH derived from SAPHIR and that derived using radiosonde observations for channels 1–3 respectively.

noise scales with the UTH value and has a relative standard deviation of approximately 7% for a radiometric noise level of 1 K (ref. 14). The weights in the definition of UTH depend on the atmospheric state; so a drier atmosphere is sampled at lower altitudes and the weighting of a specific layer of the atmosphere is not constant¹⁴.

The above methodology for the estimation of UTH has been validated with radiosonde data (RAOB) (<http://weather.uwyo.edu/upperair/sounding.html>). In the case of radiosonde data-based validation, radiosonde ascents that have measurements up to upper troposphere (100 hPa and above) have been identified from the Southeast Asian stations. Collocated level-1 SAPHIR brightness temperatures within a space widow of ± 100 km and time window

of ± 150 min are identified. The incidence angle of each collocated pixel is noted. The Jacobians at three channels are derived for the radiosonde measurements corresponding to the incidence angle of each collocated pixel for each altitude of radiosonde measurement by applying the microwave radiative transfer computation (ARTS) to radiosonde data. The weighted mean value of RH [%] (UTH) is then computed based on these Jacobians. Figure 2 shows the regression results between the radiosonde-derived UTH and that UTH from the proposed methodology (SAPHIR-UTH) for first, second and third SAPHIR channels. The results of regression and statistical analyses are tabulated in Table 3. The comparison is reasonably good with correlation coefficient of 0.6 for all the

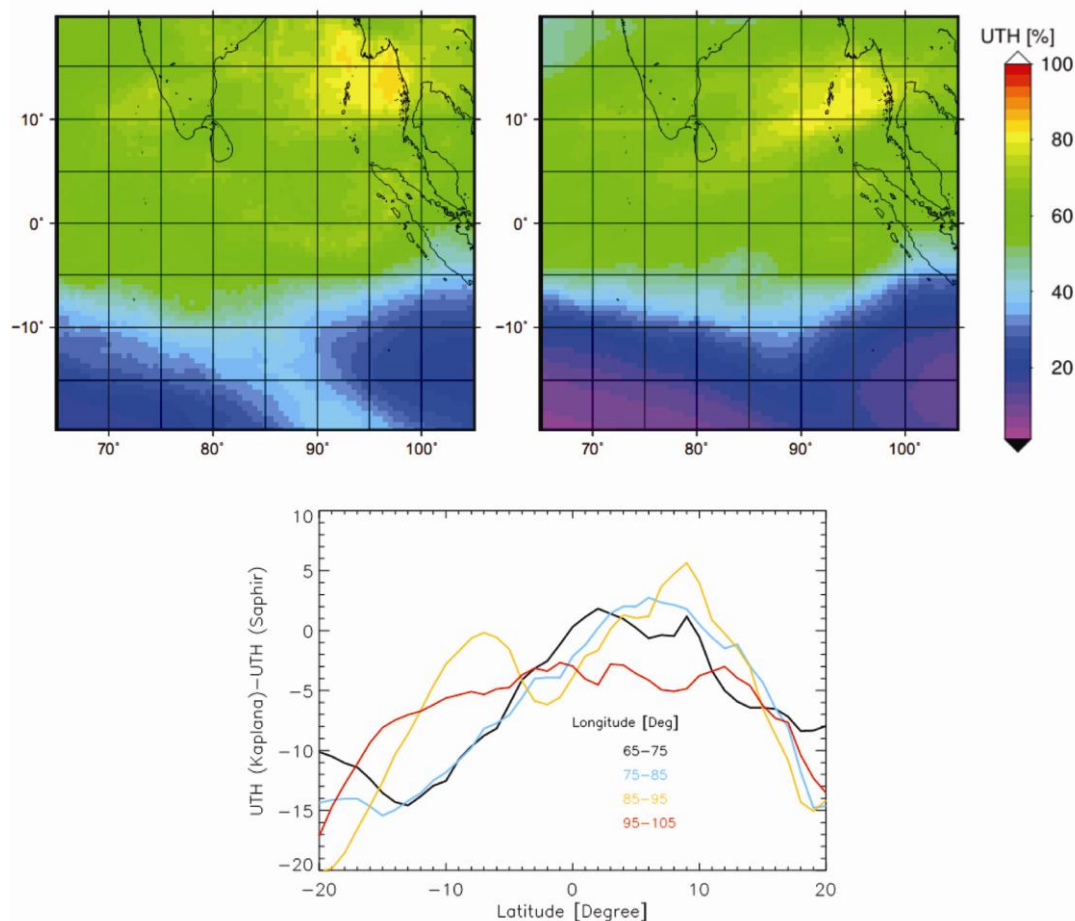


Figure 3. Comparison of UTH derived from SAPHIR (top, left) and the UTH product from Kalpana VHRR data (top, right). (Bottom) Latitudinal variation of the difference in UTH averaged for different longitudinal sectors.

Table 3. Regression parameters of the comparison of UTH derived from SAPHIR and that from RAOB

Channel no.	CC	Slope	y-intercept	Root mean square difference (%)
S1	0.64	0.4	23.4	14.0
S2	0.62	0.5	23.4	7.0
S3	0.60	0.6	23.6	4.2

CC, Correlation coefficient.

three channels and the root mean square difference between them is ~14%, 7% and 4% for channels 1, 2 and 3 respectively.

The SAPHIR-UTH has been compared with Kalpana UTH¹⁸. Since the weighting functions of Kalpana VHRR and those of the channels of SAPHIR are different, they have different information content also. The channel 3 UTH is the weighted average UTH of ~250–550 hPa altitude layers. Channels 1 and 2 have weighting function peaks even at higher altitudes. Therefore, a qualitative comparison is made here between the average UTH

derived from SAPHIR channel 3 for August 2012 for a region selected around peninsular India (65°–105°E and 20°S–20°N, where Kalpana also has coverage) and Kalpana UTH of the same period. Figure 3 shows the average UTH derived from SAPHIR channel 3 for August 2012 (top left panel) and the Kalpana UTH (top right panel). The bottom panel shows the latitude variation of the difference between both UTH, averaged for different longitudinal sectors. A considerable difference is seen only for latitudes below 10°S. Here the atmosphere is dry and the SAPHIR sounds deeper than the Kalpana VHRR. This may be a possible reason for higher values of SAPHIR-UTH.

Another validation has been done by comparing the SAPHIR-UTH with SAPHIR layer averaged humidity product. Figure 4 shows the SAPHIR-UTH for channels 1, 2 and 3 respectively (top panel); the SAPHIR layer averaged humidity product for the first three layers for the range 250–100 hPa, 400–250 hPa and 550–400 hPa respectively, for layers 1, 2 and 3 (middle panel) and their correlation plots (bottom panel). The correlation between them is 0.87, 0.97 and 0.98 respectively, for panels

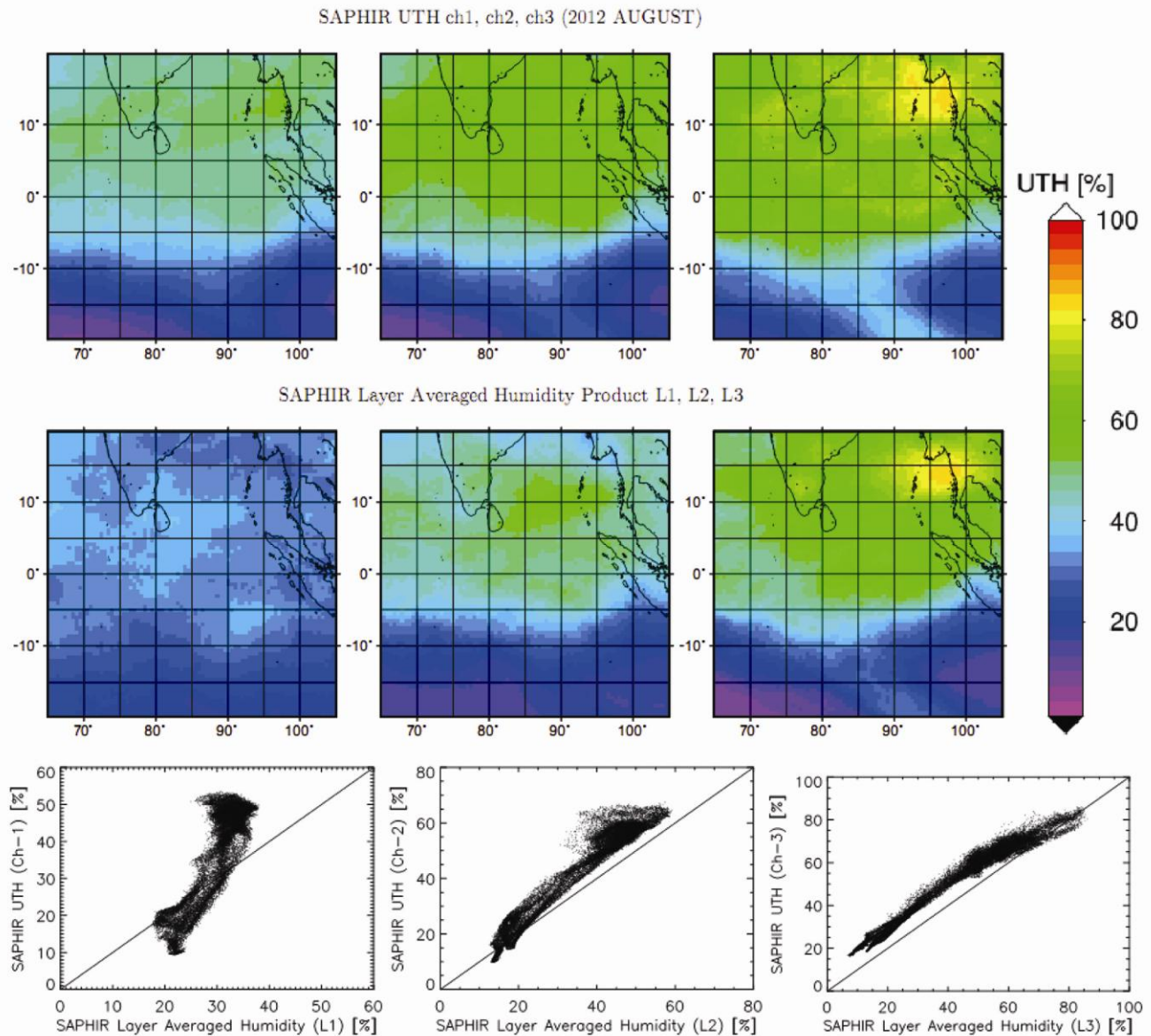


Figure 4. SAPHIR-UTH (top panel, channels 1–3), layer averaged humidity product from SAPHIR (middle panel, layers 1–3) for August 2012 and correlation between SAPHIR-UTH and the layer averaged humidity product from SAPHIR (bottom panel).

1, 2 and 3 and the corresponding mean absolute difference is 10.36, 8.4 and 7.6 respectively. The first panel (for channel 1 and layer 1) has maximum difference. Here, the altitude of averaging is 250–100 hPa for the layer average humidity product. However, in the case of SAPHIR-UTH, the weighting functions have not shown any significant values above 150 hPa. This may be a possible reason for the difference.

Figure 5 shows the global maps of layer averaged UTH for channel 1 at $0.25^\circ \times 0.25^\circ$ grid resolution from July to December 2012. The UTH in this altitude region varies from 5% to 60% in the tropical region. The region associated with deep convection in the inter-tropical convergence zone (ITCZ) exhibits high UTH values. The

regions of very low humidity correspond to the high pressure regions in the descending arm of the overturning Hadley circulation over the South Pacific, North Pacific (Pacific high), North Atlantic (Bermuda high), South Atlantic, Indian Ocean and Australia. In the band with high UTH around the ITCZ, there are three regions with significantly high humidity, one each over Central Africa, the maritime region between South Asia and Australia, and Central America. All these three are the strongest convective regions, responsible for transport of a large amount of moist air into the upper troposphere. Seasonal variation is clear in the subsequent panels. During the boreal summer, the northern hemisphere is relatively more humid compared to the southern hemisphere. A gradual

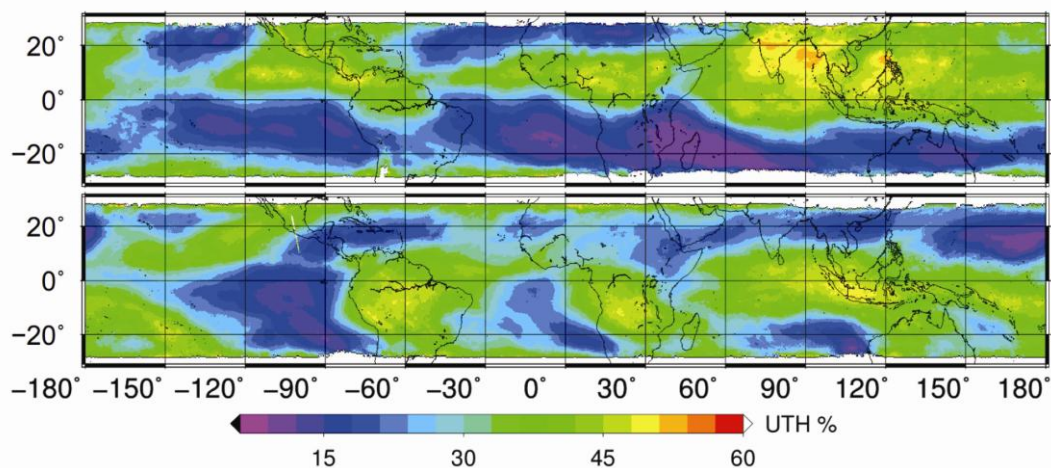


Figure 5. Spatial distribution of monthly mean relative humidity (% RH) derived from 183.31 ± 0.2 GHz from July (top panel) to December (bottom panel) of 2012.

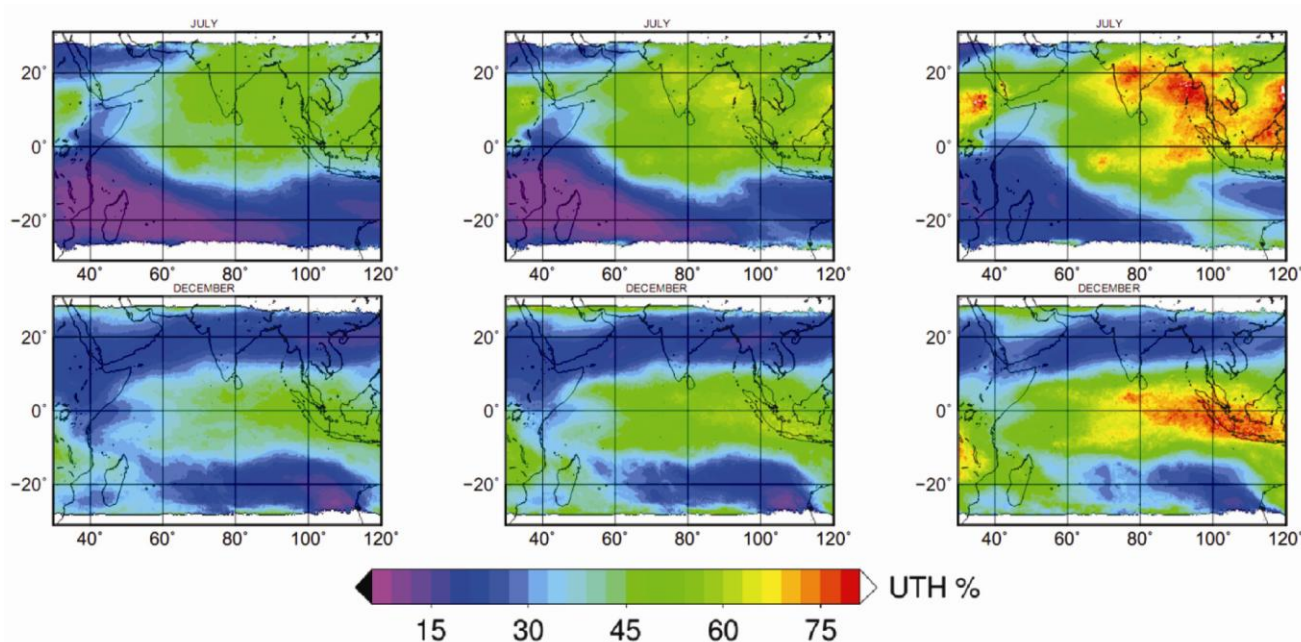


Figure 6. Average UTH (% RH) over the Indian peninsula and adjoining regions for July (top panel) and December (bottom panel) 2012. (Left column) Humidity derived from 183.31 ± 0.2 GHz; (middle column) Humidity derived from 183.31 ± 1.1 GHz; (right column) Humidity derived from 183.31 ± 2.8 GHz.

migration of humidity towards the south can be observed in the subsequent months, reflecting the southward migration of the ITCZ.

The standard deviation of UTH (% RH) corresponding to the monthly mean value was also analysed on a global basis, to indicate the day-to-day variations in UTH. Maximum variability in July was observed over the Pacific region and minimum variability over Madagascar. However, in December, though large variability was observed over the Pacific and North Atlantic regions, the low variability region had shifted to the Southwest Pacific (not shown).

The Indian subcontinent and its surrounding oceanic regions experience summer monsoon during June to September, characterized by extensive rainfall and cloudy skies. Detailed analysis has been carried out to study the Indian peninsular region and its surrounding oceanic regions. During the summer monsoon period moisture-bearing winds sweep into the continent from the ocean. Maximum UTH is observed over and around the Indian peninsular region during these months⁸. During July, the upper troposphere in the Indian and Myanmar regions is highly humid (more than the Indonesian region, where the descending limb of the walker cell is located). The

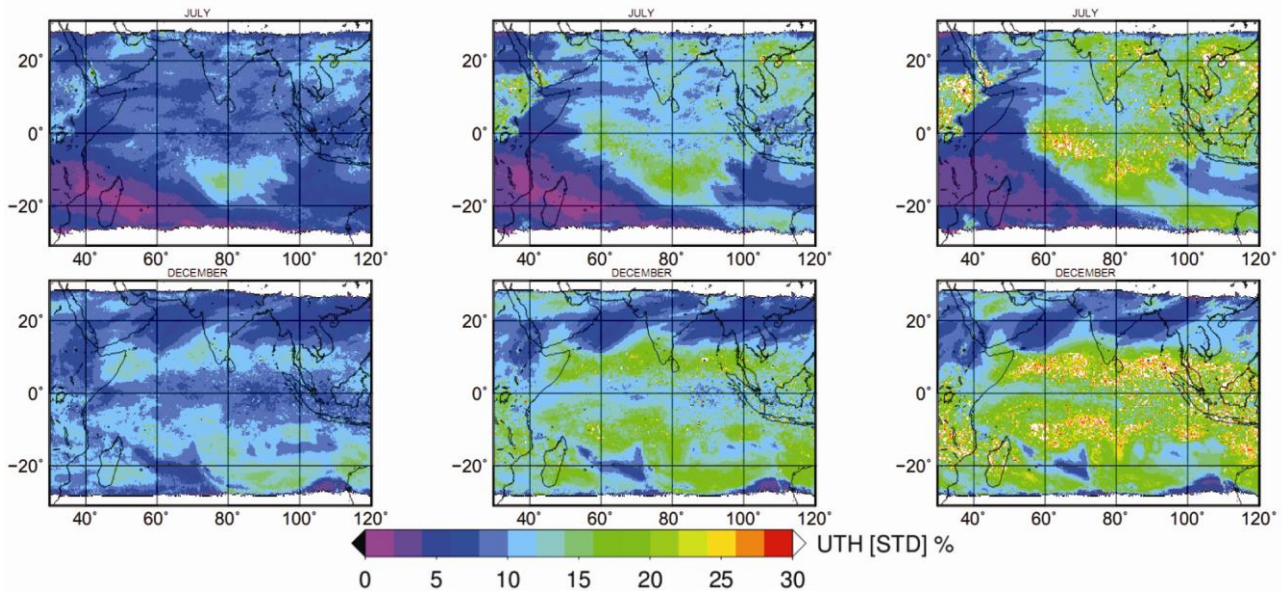


Figure 7. Same as Figure 6, but for the standard deviation of UTH (% RH) in different layers of the upper troposphere.

spatial extent of this high UTH region decreases from September and moves south (with the receding of Asian monsoon), finally being confined to the Indonesian region by boreal winter.

Figure 6 shows the average UTH (% RH) over the Indian peninsula and adjoining oceanic regions for July (top panel) and December (bottom panel) of 2012 at different altitudes. The left column represents the humidity derived from 183.31 ± 0.2 GHz, the middle column is for the humidity derived from 183.31 ± 1.1 GHz, and the right column for the humidity derived from 183.31 ± 2.8 GHz. The most important feature observed in this region is the high humidity value extending over a wide geographical region between the equator and 20°N over the Indian Ocean associated with the Indian summer monsoon during July. The area encompassed by the high humidity region in the middle troposphere (third column) is greatest during July and begins to move south in September. It further weakens, moves southward and becomes focused over the Indonesian region by November–December. It is interesting to note that the humidity content in the upper troposphere (first and second columns) is greatest over the head Bay of Bengal (BoB) region during July–September. This confirms the finding of Meenu *et al.*¹⁹. Another important feature of UTH in Figure 6 is a relatively dry region around the tip of the Indian peninsula and Sri Lanka during the monsoon period. In July, the high humidity region in the middle troposphere (third column) encompasses a relatively low humidity region between the equator and 10°N at 70° – 85°E . This is the region of inhibited cloudiness resulting from a large-scale surface divergence²⁰. The double ITCZ structure^{21,22} is also feebly seen in the middle tropospheric humidity during November and December 2012.

Figure 7 shows the standard deviation of UTH at different levels in different months during the study period. The variability of middle tropospheric humidity is small over Indian region during the monsoon period. In November and December, the high variability region gets aligned to around 5°N and 10°S with a low variability (and high UTH) region centred around the equator (only July and December are shown).

Thus, UTH at different levels are derived from the first three channels of Megha-Tropics SAPHIR brightness temperature data. The T_b to UTH transformation coefficients for the three upper tropospheric layers for all incidence angles are estimated. These transformation coefficients and the methodology to find cloud-free pixels have been presented, so that users can directly derive UTH from SAPHIR brightness temperature data. The methodology has been validated by comparing the SAPHIR-derived UTH with that derived from RAOB. The layer averaged UTH product has also been compared with Kalpana UTH. SAPHIR gives UTH at the highest possible altitude using the present microwave nadir-viewing techniques. The derived UTH depicts all gross and general features of atmospheric circulation. This high-resolution UTH will help to study several diurnally varying tropical weather features, as well as to develop diurnally unbiased humidity climatology.

1. Roca, R., Guzman, R., Lemond, J., Meijer, J., Picon, L. and Brogniez, H., Tropical and extra-tropical influences on the distribution of free tropospheric humidity over the inter-tropical belt. *Surv. Geophys.*, 2012; doi:10.1007/s10712-011-9169-4.
2. Kiehl, J. T. and Briegleb, B. P., Comparison of the observed and calculated clear sky greenhouse effect: implication for climate studies. *J. Geophys. Res.*, 1992, **97**, 10037–10049.

3. John, V. O., Holl, G., Allan, R. P., Buehler, S. A., Parker, D. E. and Soden, B. J., Clear sky biases in satellite infrared estimates of upper tropospheric humidity and its trends. *J. Geophys. Res.*, 2011, **116**(D05205); doi:10.1029/2010JD014192.
4. Soden, B. J. and Bretherton, F. P., Upper tropospheric relative humidity from the goes 6.7 μm channel: method and climatology for July 1987. *J. Geophys. Res.*, 1993, **98**(D9), 16669–16688.
5. Soden, B. J. and Fu, R., A satellite analysis of deep convection, upper tropospheric humidity, and greenhouse effect. *J. Climate*, 1995, **8**, 2333–2351.
6. Buehler, S. A., Eriksson, P., von Engel, A. and Verden, C., Arts, the atmospheric radiative transfer simulator. *Q. J. R. Meteor. Soc.*, 2005, **91**(1), 65–93; doi:10.1029/2004JD005111.
7. Buehler, S. A., John, V. O., Milz, M., Soden, B. J., Jackson, D. L. and Notholt, J., An upper tropospheric humidity data set from operational satellite microwave data. *J. Geophys. Res.*, 2008, **113**(D14110).
8. Xavier, P. K., John, V. O., Buehler, S. A., Ajayamohan, R. S. and Sijikumar, S., Variability of Indian summer monsoon in a new upper tropospheric humidity data set. *Geophys. Res. Lett.*, 2010, **37**(L05705).
9. Gohil, B. S., Gairola, R. M., Mathur, A. K., Varma, A. K., Mahesh, C., Gangwar, R. K. and Pal, P. K., Algorithms for retrieving geophysical parameters from the MADRAS and SAPHIR sensors of the Megha-Tropiques satellite: Indian scenario. *Q. J. R. Meteor. Soc.*, 2012; doi:10.1002/qj.2041.
10. Raju, G., Engineering challenges in the Megha-Tropiques satellite. *Curr. Sci.*, 2013, **104**(12), 1662–1670.
11. Suresh Raju, C., Antony, T., Mathew, N., Uma, K. N. and Moorthy, K. K., MT-MADRAS brightness temperature analysis for terrain characterization and land surface microwave emissivity estimation. *Curr. Sci.*, 2013, **104**(12), 1643–1649.
12. Eymard, L. *et al.*, The SAPHIR humidity sounder, Megha-Tropiques 2nd Scientific Workshop, Paris, France, 2–6 July 2011.
13. Chaboureau, J. P., Chedin, A. and Scott, N. A., Remote sensing of the vertical distribution of water vapor from the TOVS observations: method and validation. *J. Geophys. Res.*, 1998, **103**(D8), 8743–8752.
14. Buehler, S. A. and John, V. O., A simple method to relate microwave radiances to upper tropospheric humidity. *J. Geophys. Res.*, 2005, **110**(D02110); doi:10.1029/2004JD005111.
15. Melsheimer *et al.*, Inter-comparison of general purpose clear sky atmospheric radiative transfer models for the millimeter/submillimeter spectral range. *Radio Sci.*, 2005, **40** (RS1007); doi:10.1029/2004RS003110.
16. Hong, G., Heygster, G. and Kunzi, K., Detection of tropical deep convective clouds from AMSU-B water vapor channels measurements. *J. Geophys. Res.*, 2005, **110**(D05205), 1–15.
17. Burns, B. A., Wu, X. and Diak, G. R., Effects of precipitation and cloud ice on brightness temperature in AMSU moisture channels. *IEEE Trans. Geosci. Remote Sensing*, 1997, **5**(6), 1429–1437.
18. Thapliyal, P. K., Shukla, M. V., Shah, S., Pal, P. K., Joshi, P. C. and Kottayil, A., An algorithm for the estimation of upper tropospheric humidity from Kalpana observations: methodology and validation. *J. Geophys. Res.*, 2011, **116**, 1–16; doi:10.1029/2010JD014291.
19. Meenu, S., Rajeev, K., Parameswaran, K. and Nair, A. K. M., Regional distribution of deep clouds and cloud top altitudes over the Indian subcontinent and the surrounding oceans. *J. Geophys. Res.*, 2010, **115**(D05205); doi:10.1029/2009JD011802.
20. Nair, A. K. M., Rajeev, K., Sijikumar, S. and Meenu, S., Characteristics of a persistent pool of inhibited cloudiness and its genesis over the Bay of Bengal associated with the Asian summer monsoon. *Ann. Geophys.*, 2011, **29**(4), 1247–1252.
21. Zhang, C., Double ITCZ. *J. Geophys. Res.*, 1993, **106**, 11785–11792.
22. Meenu, S., Rajeev, K., Parameswaran, K. and Suresh Raju, C., Characteristics of the double inter-tropical convergence zone over the tropical Indian ocean. *J. Geophys. Res.*, 2007, **112**(D11106); doi:10.1029/2006JD007950.

ACKNOWLEDGEMENTS. We thank Dr Parameswaran and Dr K. Rajiv, Space Physics Laboratory, Vikram Sarabhai Space Centre, Thiruvananthapuram for fruitful discussions and careful reading of the manuscript. We also thank MOSDAC, SAC for supplying the SAPHIR data and humidity products (<http://mosdac.gov.in>). V.O.J. was supported by the joint DECC/Defra Met Office Hardley Centre Climate Programme (GA01101), the UK JWCPR and EUMETSAT CMSAF. Radiosonde data are from <http://weather.uwyo.edu/upperair/sounding.html>.

Received 12 September 2014; revised accepted 23 March 2015

Indian and Chinese higher education institutions compared using an end-to-end evaluation

S. Savithri* and Gangan Prathap

CSIR-National Institute for Interdisciplinary Science and Technology, Thiruvananthapuram 695 019, India

The latest (2014) release of the SCImago Institutions Rankings (SIR) allows to compare the research performance of leading higher education institutions in India and China using an end-to-end bibliometric performance analysis procedure. Six carefully chosen primary and secondary bibliometric indicators summarize the chain of activity: input–output–excellence–outcome–productivity. From principal component analysis it is established that the primary indicators are orthogonal and represent size-dependent quantity and size-independent quality/productivity dimensions respectively. Using this insight two-dimensional maps can be used to visualize the results.

Keywords: Bibliometrics indicators, higher education institutions, principal component analysis, research performance.

BOTH in India and China, the higher education institutions (HEIs) taken together are the key contributors to their academic research output. HEIs constitute 19 out of the top 20 research entities in China, and 15 out of the top 20 in India according to the latest SCImago Institutions Rankings (SIR) World Reports (<http://www.scimagoir.com/>). Overall there are 391 HEIs from China and 156 from India in the SIR list for 2014. Most of these can be considered as significantly research-intensive. So far, the

*For correspondence. (e-mail: sivakumarsavi@gmail.com)